

Pittsburg State University

Pittsburg State University Digital Commons

Electronic Theses & Dissertations

Spring 2-12-2021

COMBINATION THERAPY: DUAL DRUG-LOADED SUPERPARAMAGNETIC IRON-OXIDE NANOPARTICLE FOR TARGETED DRUG DELIVERY AND TREATMENT OF CANCER

Himanshu Polara

Pittsburg State University, hpolar@pittstate.edu

Follow this and additional works at: <https://digitalcommons.pittstate.edu/etd>

 Part of the [Chemistry Commons](#)

Recommended Citation

Polara, Himanshu, "COMBINATION THERAPY: DUAL DRUG-LOADED SUPERPARAMAGNETIC IRON-OXIDE NANOPARTICLE FOR TARGETED DRUG DELIVERY AND TREATMENT OF CANCER" (2021). *Electronic Theses & Dissertations*. 474.

<https://digitalcommons.pittstate.edu/etd/474>

This Thesis is brought to you for free and open access by Pittsburg State University Digital Commons. It has been accepted for inclusion in Electronic Theses & Dissertations by an authorized administrator of Pittsburg State University Digital Commons. For more information, please contact digitalcommons@pittstate.edu.

COMBINATION THERAPY: DUAL DRUG-LOADED SUPERPARAMAGNETIC IRON-
OXIDE NANOPARTICLE FOR TARGETED DRUG DELIVERY AND TREATMENT OF
CANCER

A Thesis Submitted to the Graduate School
in Partial Fulfillment of the Requirements
for the Degree of
Master of Science in Chemistry

Himanshu Polara

Pittsburg State University

Pittsburg, Kansas

February 2021

COMBINATION THERAPY: DUAL DRUG-LOADED SUPERPARAMAGNETIC IRON-
OXIDE NANOPARTICLE FOR TARGETED DRUG DELIVERY AND TREATMENT OF
CANCER

Himanshu Polara

APPROVED:

Thesis Advisor

Dr. Santimukul Santra, Department of Chemistry

Committee Member

Dr. William Shirley, Department of Chemistry

Committee Member

Dr. Irene Zegar, Department of Chemistry

Committee Member

Dr. Virginia Rider, Department of Biology

ACKNOWLEDGMENTS

I want to express my gratitude to my research mentor Dr. Santimukul Santra, who gave me a golden opportunity to work under his guidance. Dr. Santra knows my abilities and career goals, so he designed an appropriate project to fulfill my life goals. I would also like to thank the "Nanotheranostic lab" for allowing me to work in the lab throughout my master's program.

I would like to thank all my family members and friends for supporting me. Special thanks go to Sarthi, my best friend, wife, girlfriend, for always believing in me and encouraging me to finish my dreams.

I am grateful to all my lab members for believing in me and support me in my personal and academic life. I would like to thank the chemistry and biology departments for giving me the best education and research experience.

COMBINATION THERAPY: DUAL DRUG-LOADED SUPERPARAMAGNETIC IRON-OXIDE NANOPARTICLE FOR TARGETED DRUG DELIVERY AND TREATMENT OF CANCER

An Abstract of the Thesis by
Himanshu Polara

Lung cancer is the most occurring form of cancer of all ages in the United States after breast cancer. Many treatments are currently available in the market to treat cancer, but they all have some side effects. The concept of nanomedicine-based targeted drug delivery has been developed to overcome the limitations of current treatment. The advantages of this method of treatment include biocompatibility, significant toxicity towards cancer cells, immediate drug response, and fewer side effects. For the specific treatment of A549 lung cancer cells, polyacrylic acid (PAA) coated Iron Oxide Nanoparticle (IONP) was introduced for magnetic resonance imaging (MRI) of lung cancer. To make these nanoparticles specifically target A549 cells, a folate receptor targeting ligand was conjugated on the surface through carbodiimide chemistry. The novel approach of combining two drugs, doxorubicin and fingolimod, was designed for this study. Drugs were co-encapsulated within the PAA coating of Magnetic Nanoparticles (MNPs) by the solvent diffusion method. Doxorubicin was encapsulated with MNPs to target the tumor cells to compare the synergistic effect of combination therapy on a tumor site at different time-points. Significant synergistic cell killing was accomplished in doxorubicin and fingolimod dual drug-loaded vesicles in lung cancer cells. This combination therapy's therapeutic efficacy over a single drug usage was confirmed using several cell-based assays such as a comet, ROS, cell migration, and apoptosis.

TABLE OF CONTENTS

CHAPTER	PAGE
I. INTRODUCTION.....	01
II. RESULTS AND DISCUSSION.....	12
III. EXPERIMENTAL SECTION.....	22
IV. CONCLUSION AND FUTURE STUDY.....	25
REFERENCES.....	26

LIST OF FIGURES

Chapter I

Figure 1. The estimation of new cancer cases and deaths for ten leading cancers by sex in the United States in 2020.....	2
Figure 2. Nanocarrier HBPE with conjugated folate and diethylenediamine.....	4
Figure 3. Dose- and time-dependent cytotoxicity assay of prostate cancer cells.....	5
Figure 4. Graphical demonstration of gold nanoparticles at tumor sites.....	6
Figure 5. Different types of gold nanoparticles in drug delivery system.....	6
Figure 6. ICP-MS of silica concentration in each organ of mice with xenograft tumors.....	7
Figure 7. Fluorescence spectra of doxo-TCL-SPION and doxo-TCL-SPION-Apt.....	8
Figure 8. Cell proliferation assay in LNCaP and PC3 cells.....	9
Figure 9. Schematic demonstration of combination approach to A549 lung cancer cells.....	10
Figure 10. Structural formula of doxorubicin and fingolimod.....	11

Chapter II

Figure 11. Synthesis of folate conjugated, and drugs encapsulated IONPs for the treatment.....	13
Figure 12. Characterization of carboxyl IONPs.....	14
Figure 13. Characterization of drug encapsulated IONPs.....	15
Figure 14. Characterization of folate conjugated, and drug loaded IONPs.....	16
Figure 15. Time dependent MTT assay of A549 cells.....	17
Figure 16. Time dependent MTT assay of CHO cells.....	18
Figure 17. ROS generation assay.....	19
Figure 18. Cellular apoptosis assay.....	20
Figure 19. Migration assay.....	21

LIST OF ABBREVIATIONS

IONPs: Iron oxide nanoparticles

IONP-COOH: Carboxyl iron oxide nanoparticles

PAA: Polyacrylic acid

Doxo: Doxorubicin

Fingo: Fingolimod

EDC: 1-ethyl-3-(3-dimethylaminopropyl) carbodiimide)

NHS: N-hydroxy succinimide

DMSO: Dimethyl sulfoxide

MTT: (3-(4, 5-dimethyl-thiazol-2-yl)-2, 5 diphenyl tetrazolium bromide)

PBS: Phosphate buffer saline

FBS: Fetal bovine serum

DAPI: 4',6-diamidino-2-phenylindole

MRI: Magnetic resonance imaging

DLS: Dynamic light scattering

DHE: Dihydroethidium

EDA: Ethylenediamine

Chapter I

Introduction

Cancer is a significant public health concern and the second most common leading cause of death globally. According to the American Cancer Society (ACS), lung cancer accounts for an estimated 1.8 million new cases and 606,520 deaths in the United States in 2020.¹ A survey taken by the world health organization shows that cancer-related death is expected to be nearly 12 million worldwide by 2030.² There are various types of cancer, such as breast cancer, prostate cancer, thyroid cancer, colorectal cancer; however, in this study, the main focus was the lung cancer. After indicating all these statistics of deaths worldwide, scientists came up with various treatments to treat lung cancer. Current treatments include surgery, radiation, chemotherapy, and hormone therapy for any cancer. Although these regular treatments improve a cancer patient's survival rate, they cause damage and become toxic to normal cells because of the non-specific distribution of drugs, causing adverse side effects such as hair loss, weakness, and nausea.³ To overcome this limitation, nanomedicine has been of significant interest over the decades as it can simultaneously carry both; drugs and imaging probes, and through this, specific targetability is achieved to avoid damage to healthy tissue. The presence of a functional group on the surface of nanoparticles is used to conjugate drugs for targeted drug delivery to the tumor.

Lung cancer is most common in active smokers, and people who may have never smoked have a risk of getting lung cancer.² Lung cancer is predominantly classified into two different types: non-small cell lung cancer (NSCLC) and small cell lung cancer (SCLC). NSCLC accounts for 85% of lung cancer deaths due to the scarcity of timely detection of NSCLC.⁴ Whereas, SCLC is less common and accounts for the rest of the 15% of lung cancer. Adenocarcinoma (ADC) is one of the most usual histological subtypes of NSCLC.^{5,6} Acute side effects, multidrug endurance, and low survival rate are restrictions for the prevailing NSCLC treatment; thus, urgency in developing an effective treatment arises for NSCLC. Platinum-based combination chemotherapy demonstrates the usual care of patients with NSCLC, improving lung cancer's overall survival rate.⁷⁻⁹ The most common cancer types with estimated new cases and deaths in 2020 are shown in figure 1. As seen

in **figure 1**, prostate and lung cancer are most common in males accounting for 34% of total cases. Whereas breast and lung, cancer accounts for 42% of total cases in females.¹⁰

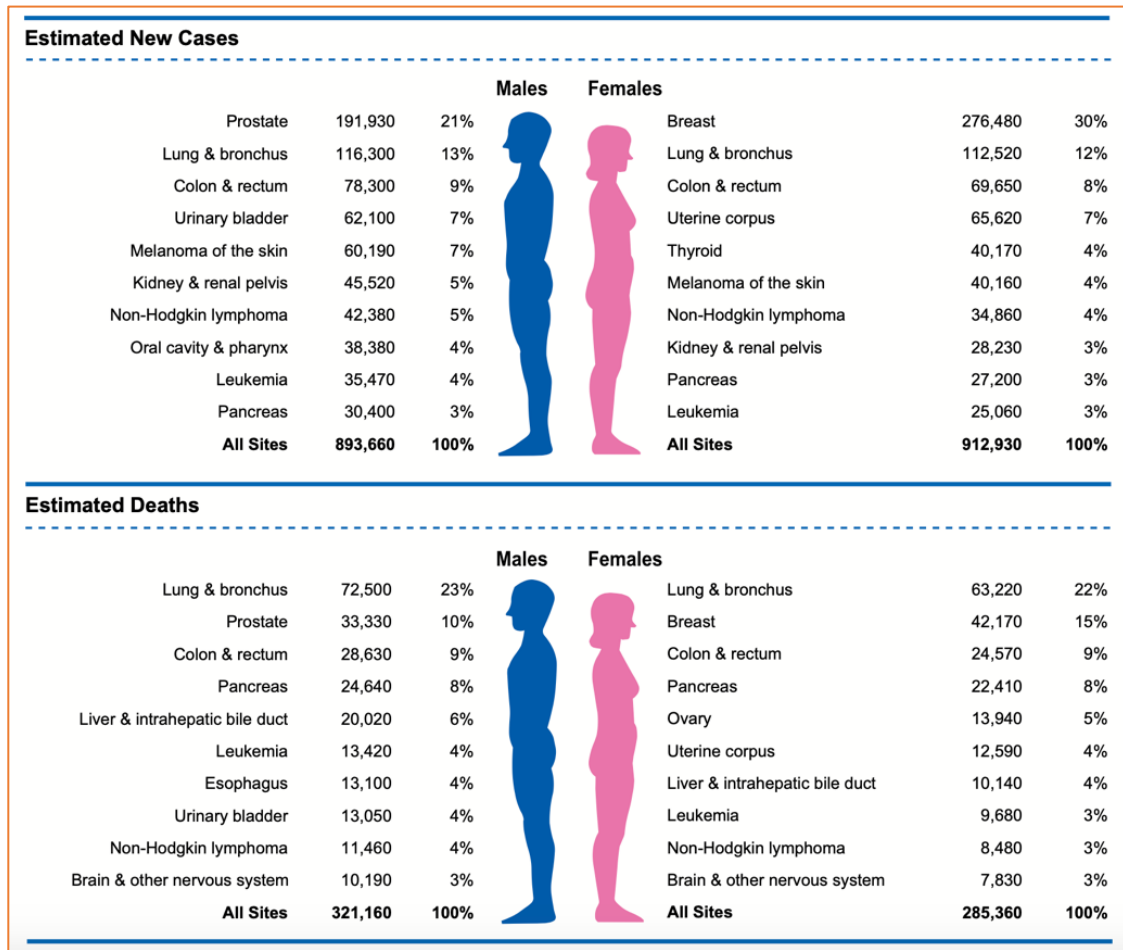


Figure 1: The estimation of new cancer cases and deaths for ten leading cancers by sex in the United States in 2020. These estimated figures were rounded to the nearest ten and exclude basal cell and squamous cell skin cancers and in situ carcinoma except for urinary bladder. The ranking is based on modeled projections and might differ from the most recent observed data.¹⁰

1) Nanotechnology: A better way of treatment

Over the five decades, chemotherapy has been used as a primary treatment to cure any cancer. In this non-specific treatment, the drug attacks the tumor site, attacks normal cells and causes side effects. To overcome the limitation, scientists need to determine how the drug goes specifically to the tumor site. The recent development in cancer shows that nanotechnology played a vital role in the drug delivery system. Therapeutic nanoparticles (NPs) that can precisely target and deliver drugs without causing damage to normal cells have been created.¹¹ Multiple NPs with

the ability to target cancer cells and release the desired anticancer drugs in a controlled and time-dependent manner were developed using targeting ligands such as amino acids, antibodies, and proteins.¹² The multimodal functionality of iron oxide nanoparticles (IONP) proves that they can be used as a contrast agent in MR imaging due to their superparamagnetic nature. Likewise, gold nanoparticles (AuNPs) have the same properties to carry and deliver anticancer drugs in cancer treatment. Various polymeric nanoparticles are also used in drug delivery as they effectively enhance the therapeutic benefits.¹³

1.1) Polymeric nanoparticles for drug delivery:

The consideration of various polymeric nanoparticles has been increasing because they play a vital role in drug delivery over the decades. Biodegradable polymers, for example, polylactic acid (PLA), polylactic-co-glycolic acid (PLGA), and polycaprolactone (PCL) and their copolymers with poly(ethylene glycol) (PEG) have been usually used to form polymeric nanoparticles (NPs) to encapsulate different types of therapeutic agents along with a surface modification to attach ligand for targeted delivery. These contain polymeric micelles, capsules, colloids, dendrimers, and so on.¹⁴⁻¹⁸

In this direction, Santra et al. introduced folate conjugated hyperbranched polyester (HBPE) nanoparticles used as a drug carrier to treat cancer.¹⁹ The HBPE nanocarrier was synthesized and encapsulated with therapeutic CT20p peptide. Polyethylene glycol (PEG) was conjugated on the surface of HBPE to minimize the non-specific binding. As shown in **figure 2A**, folic acid was linked to HBPE using ethylenediamine as a linker. **Figure 2B** shows a STEM image indicating Folate-HBPE CT20p is nearly 80 nm in size, fulfilling the definition of a nanoparticle. The time and pH-dependent release profile of CT20p peptide shown in **figure 2C**.

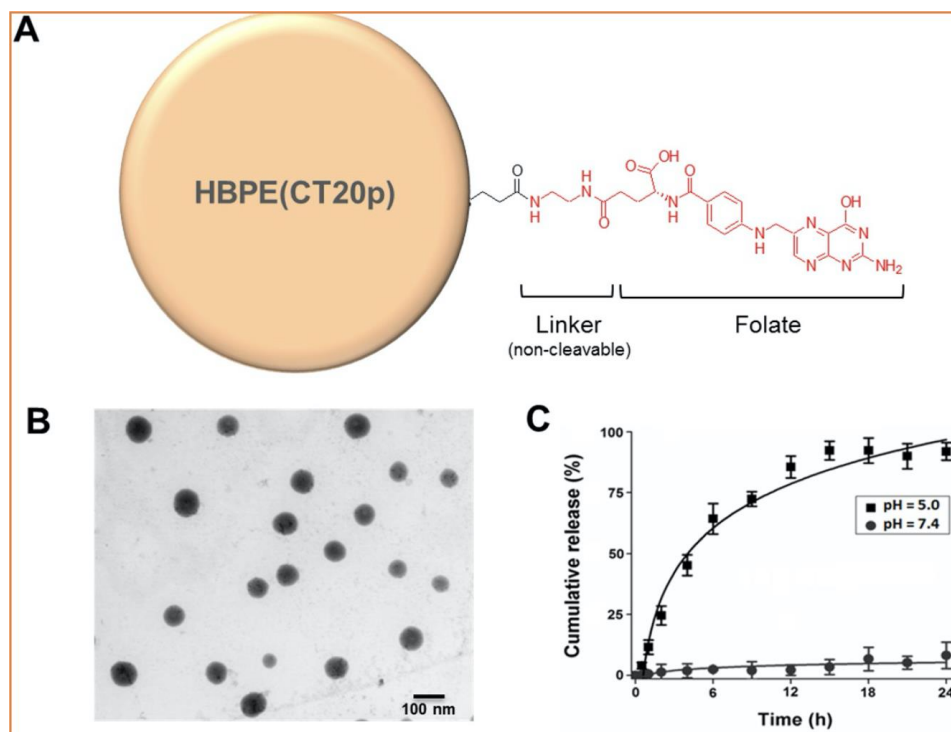


Figure 2: (A) Nanocarrier HBPE (CT20p) with conjugated folate and diethylenediamine as a linker. (B) Scanning transmission electron micrograph (STEM) image of the nanocarrier. (C) CT20p peptide release profile from HBPE nanoparticle at pH 5.0 and 7.4.¹⁹

The protonation of the carboxylic group of polymer makes a disturbance between hydrogen bonding and van der Waals interaction that is initializing release at acidic pH.¹⁹ As seen in **figure 3A**, cell viability was measured when LNCaP cells were treated with various concentrations ranging from 0-12 nM. After incubating LNCaP cells with folate HBPE and folate-HBPE(CT20p), results showed more than 80% cell death achieved with 6 nM concentration of peptide (**Figure 3D**) in 48 h. **Figure 3B,E** demonstrated that PSMA (+) PC3 cells treated with drugs showed practically the same response as LNCaP cells. PC3 cells are PSMA (-), thus resulted in no cytotoxicity as usual (**Figure 3C, 3F**).¹⁹

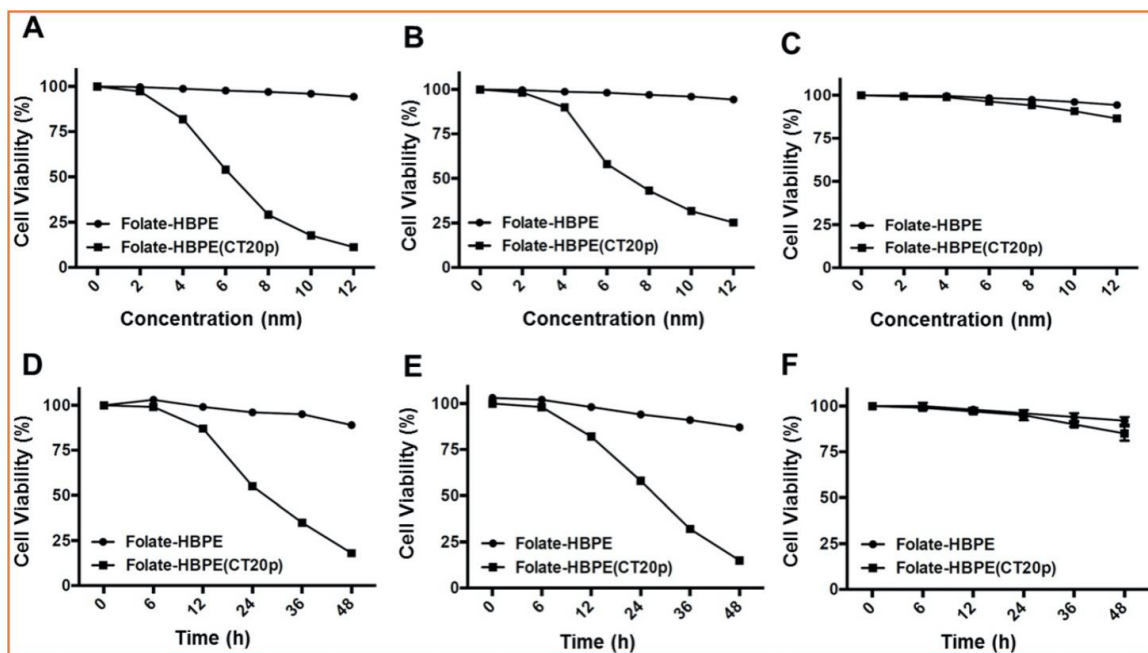


Figure 3: Dose- (a–c) and time- (d–f) dependent cytotoxicity assay (MTT) of prostate cancer cells treated with Folate HBPE(CT20p)-NPs and Folate-HBPE. LNCaP cells (A,D) PSMA (+) PC3 (B,E) and PC3 cells (C,F).¹⁹

1.2) Gold nanoparticles for drug delivery:

Michael Faraday found the ruby gold nanoparticles (Au-NPs), which turned into the establishment for advanced nanotechnology.²⁰⁻²² Mie tried to find out the different colors of gold colloids.²³ Lately, the uses of Au-NPs stretched into different bio-clinical fields, for example, photo thermolysis, biosensors, immunoassays, clinical science, genomics, microorganisms recognition and control, optical imaging, and checking of biological cells and tissues by scattering, and targeted drug delivery.²⁴⁻²⁷

Gold nanoparticles have unique characteristics such as surface modification, imaging, and proposing gold nanoparticles to apply to anticancer drug carriers.²⁸ In healthy cells, the vascular endothelial film is highly attached and arranged in such a manner that prevents the passage of fragments. Neovasculatures are formed with tumor advancement and are considered a highly disordered vascular endothelial layer with large gaps between tissues, resulting in leaks and susceptibility for the passage of particles.²⁹ Molecule of specific sizes, such as liposomes, nanoparticles are found more in cancerous tissue than the healthy tissue, called the enhanced permeability and retention (EPR) effect.³⁰⁻³² Due to the EPR effect of nanoparticles' growth in solid tumor sites by inactive targeting, NPs act as a drug carrier and demonstrate a substantial impact on tumor sites and fewer theragnostic effects on healthy organs (**Figure 4**).

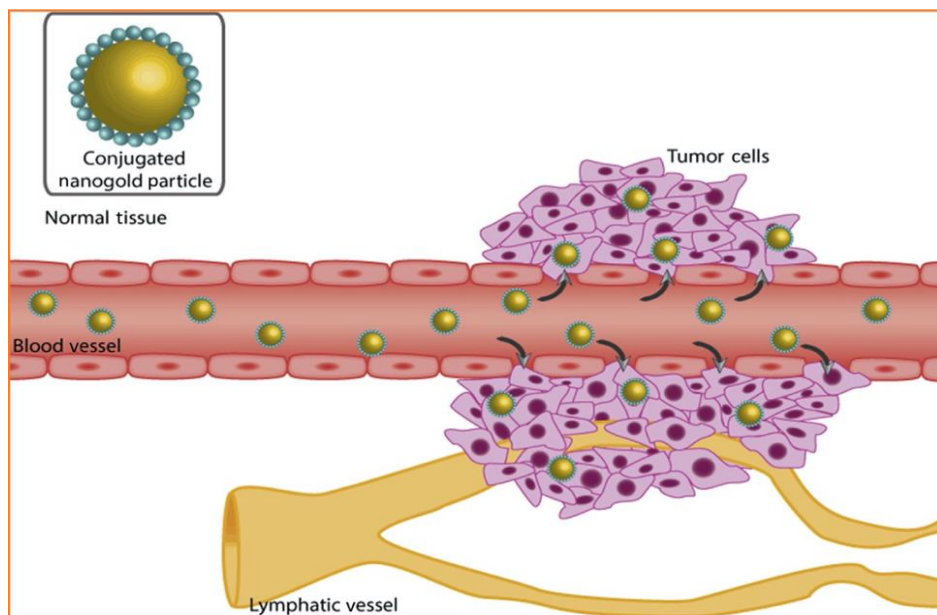


Figure 4: Graphic demonstrating the accumulation of circulating gold nanoparticle conjugates at tumor sites by the enhanced permeability and retention effect.²⁹



Figure 5: Different types of gold nanoparticles commonly used in the anticancer diagnosis and therapeutic applications shown.²⁹

Besides size and surface chemistry, the shape of the nanoparticle is the main factor for cellular uptake. For example, spherical gold nanoparticles show more absorption than rod-shaped gold nanoparticles.³³ Gold nanoparticles are available in various surface sizes ranging from 1 nm to 150 nm (**Figure 5**); thus, GNPs can easily modify in a controlled manner for drug release study.

1.3) Silica nanoparticles for drug delivery:

Recent developments in the field of surface functionalization of inorganic nanoparticle-based delivery vehicles, like mesoporous silica nanoparticles (MSN), add a promising new direction for drug delivery research.³⁴ Due to their significant applications as a drug-carrier, MSNs are popular amongst different inorganic nanoparticles. The characterization of silica nanoparticles

includes wide surface area, controlled particle sizes and shape of the particles, pore size, and dual-functionalized surfaces.³⁵ The size and shape of controllable pores are useful for carrying drugs and preventing the drugs' early release before it reaches the tumor.³⁶ Caruso and his colleagues recognized an alternative approach utilizing mesoporous silica particles as templates to make submicrometer-sized polymer capsules for anticancer drug delivery.³⁷⁻³⁹

Hudson et al. reported that intravenous administration of 1.2 g kg⁻¹ MSNs is harmful to SV129 mice, but it is safe for a mouse when used in less quantity (40 mg kg⁻¹).⁴⁰ Inductively coupled plasma mass spectroscopy (ICP-MS) was performed to determine the dissemination of drugs over the organs. A mouse was injected with human breast cancer tumor and then injected with fluorescent mesoporous silica nanoparticles (FMSNs) and folic acid conjugated fluorescent mesoporous silica nanoparticles (F-FMSNs) via tail. After 4 h incubation with FMSNs, the silica concentration moved to 45 ng/mg in the tumor. In contrast, the concentration of Si varies from 3 to 20 ng/mg in other organs (**Figure 6**). Over 24 h of incubation, the concentration of Si increased by 60 ng/mg in the tumor when treated with FMSNs, while Si's concentration increased by 105 ng/mg was observed in the tumor when treated with F-FMSNs. However, folate conjugated nanoparticle F-FMSN demonstrated a high concentration of Si in the tumor, with the highest concentration detected at 24 h. In other parts of the body, a lower concentration of Si was observed. Thus, the study showed that FMSNs are biocompatible at different doses, efficient enough to diminish the toxicity of the drugs, accumulate in tumors with or without targeting, and are quick and capable of drug delivery.⁴¹

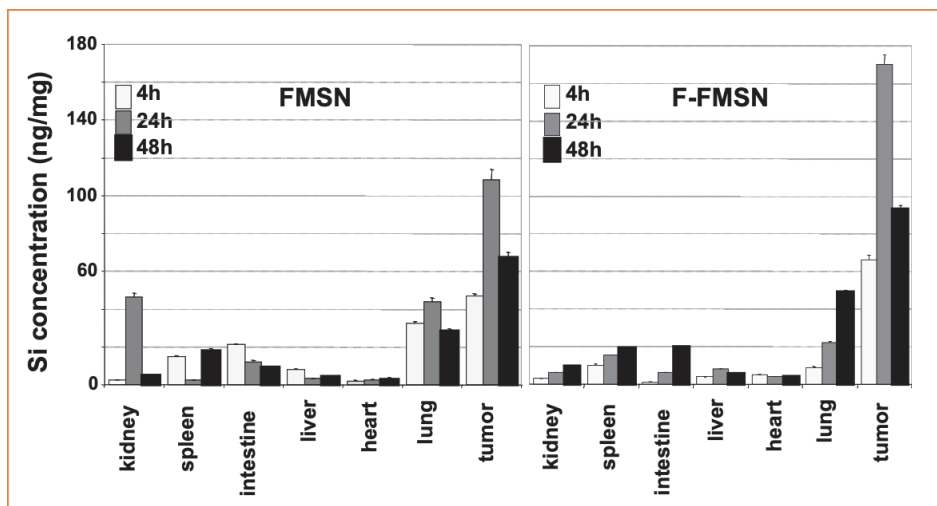


Figure 6: ICP-MS quantitative measurement of Si concentrations in each organ of the mice with xenograft tumors. The results were shown as mean values +/- SD.⁴¹

1.4) Iron oxide nanoparticles for drug delivery:

Superparamagnetic iron oxide nanoparticles (SPION) have been used for cancer treatment in the medicinal industry. IONPs become superparamagnetic when the size of the surface reached ~ 20 nm or less at room temperature.⁴² One of the most significant applications of SPION is that they are MRI contrast agents. Lee and his colleague characterize the thermally cross-linked superparamagnetic iron oxide nanoparticles (TCL-SPION) to treat cancer. Then, the dye was conjugated with TCL-SPION, which does not contain any targeting ligand. The fluorescence study demonstrated that the dye conjugated TCL-SPION was able to identify the tumor.⁴³

Wang et al. study was directed on the therapeutic agent for the treatment of cancer. In his research, they were able to characterize TCL-SPION as an MRI contrast agent. A10 RNA aptamer (Apt) binds the extracellular domain of the prostate-specific membrane antigen (PSMA) to target nanoparticles for cancer treatment and imaging. The amount of doxo that can bind to the TCL-SPION-Apt using intercalation into the aptamer and adsorption with a negatively charged NP's surface was investigated initially. The conjugation of doxo with the aptamer indicated the quenching of doxo fluorescence.⁴⁴⁻⁴⁶ A fixed amount of doxo was titrated with TCL-SPION and TCL-SPION-Apt using the Spectro fluorophotometer.

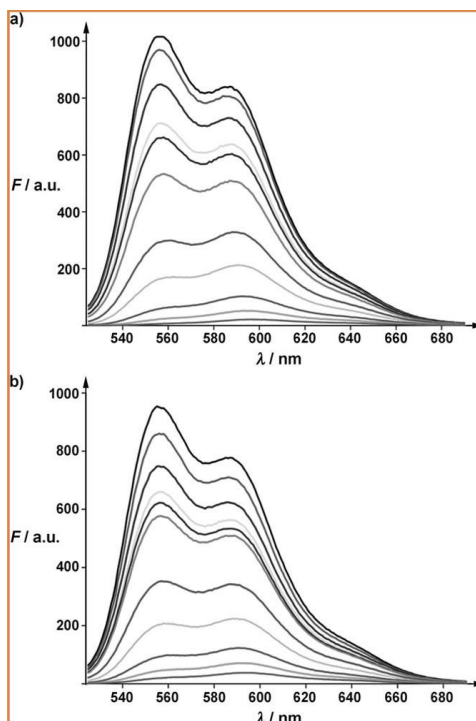


Figure 7: Fluorescence spectra of doxorubicin solution (12 mg in 0.45 mL) with increasing amounts of a) TCL-SPION (from top to bottom: 5, 15, 30, 36, 52, 100, 150, 260, 360, and 520 mg) and b) TCL-SPION–Apt (from top to bottom: 4, 13, 22, 31, 44, 88, 133, 220, 311, and 440 mg).⁴⁶

As seen in **figure 7**, the amount of TCL-SPION and TCL-SPION-Apt used to quench 12 mg of doxo were 0.52 and 0.44 mg, respectively. 85% of doxo was attached to the polymer via electrostatic interaction, and the rest of the 15% doxo was conjugated into an aptamer. Wang et al. calculated the antiproliferation activity in both LNCaP and PC3 cell lines for formulated doxo loaded nanoparticles. As seen in **figure 8**, the cytotoxicity of Apt-SPION was less potent as the control. However, free doxo demonstrated similar toxicity to both the cell lines. In comparison, TCL-SPION-Apt is considerably more effective with the PSMA targeting LNCaP cell than the non-targeted PC3 cell.⁴⁶

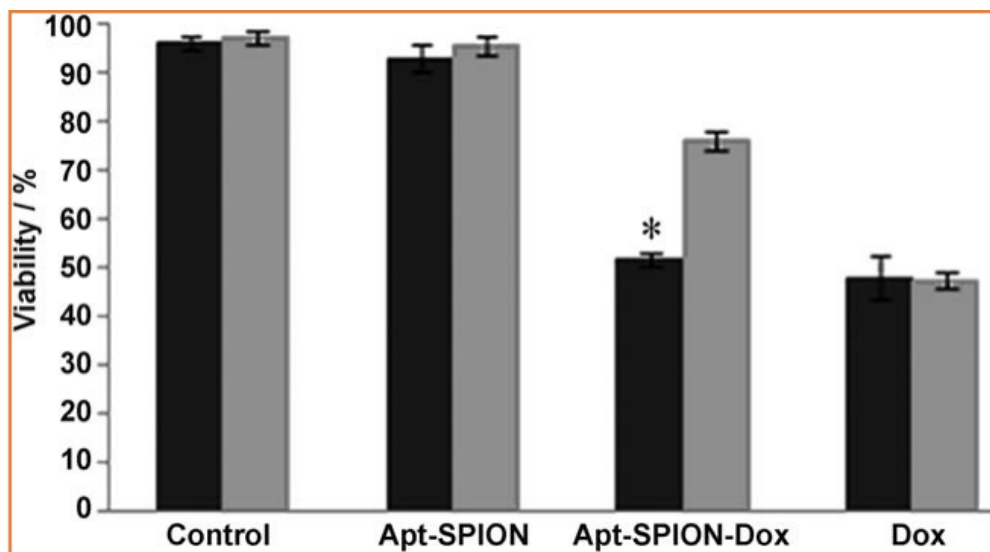


Figure 8: Cell proliferation assay for LNCaP ■ & PC3 ■ cells.⁴⁶

The ability to detect molecular changes in tumors and identify the therapeutic outcome against these targets is critically essential to treat cancer. New imaging-based magnetic resonance techniques have given a piece of new equipment to scientists to care for cancerous tumors. MRI is one of the best imaging tools available in diagnostic imaging because it allows imaging of tissue and organs and redevelops non-invasive images.⁴⁷ MRI has become a crucial technique for routine clinical diagnosis and is universally used for in vivo research.⁴⁸ Due to its numerous benefits, including short imaging times, non-invasive characteristics, signal-to-noise (S/N) ratio, and high spatial resolution, MRI has achieved significant consideration in the field of molecular imaging.⁴⁹ Molecular imaging techniques facilitate pathologic biomarker detection, thus, enhancing the diagnosis of diseases and improved therapeutic management.⁴⁷⁻⁴⁹

Inappropriate diagnostic procedures for early detection and ineffectual therapeutic strategies resulted in the harmfulness of lung cancer. The nano-size particles were introduced for

promising drug delivery for lung cancer. As discussed, different types of nanoparticle-based drug delivery systems are available in the market. However, these systems are not entirely successful for targeted delivery. Among them, IONPs shows a unique ability to hold drug and dye simultaneously. This drug delivery system enhances the therapeutic efficacy of cancer tumors and diminishes the toxicity to healthy cells.

This study synthesized nanoparticles using anticancer drugs as a multimodal MR imaging and treatment of lung cancer. IONPs encapsulated with anticancer drugs, doxorubicin and fingolimod, and then folic acid was conjugated on the surface of iron oxide nanoparticle (IONP-Folate) to attain specific targetability to lung cancer cells containing folate receptors. The mechanism of these drugs helps to acquire theranostic effect on lung cancer cells. As seen in **figure 9**, the cytotoxicity of doxorubicin is primarily due to DNA damage and fingolimod blocks the lymphocytes from going out from lymph nodes, decreasing the number of lymphocytes in the blood. Encapsulation of these drugs into IONPs shows improved drug delivery and the synergetic effect of drugs in a cancer patient. In this study, a combination of two drugs, doxorubicin (doxo) and fingolimod (fingo), for the targeted treatment of lung cancer was developed. Overall, the novel combination approach provided a synergistic effect within the lung cancer cells.

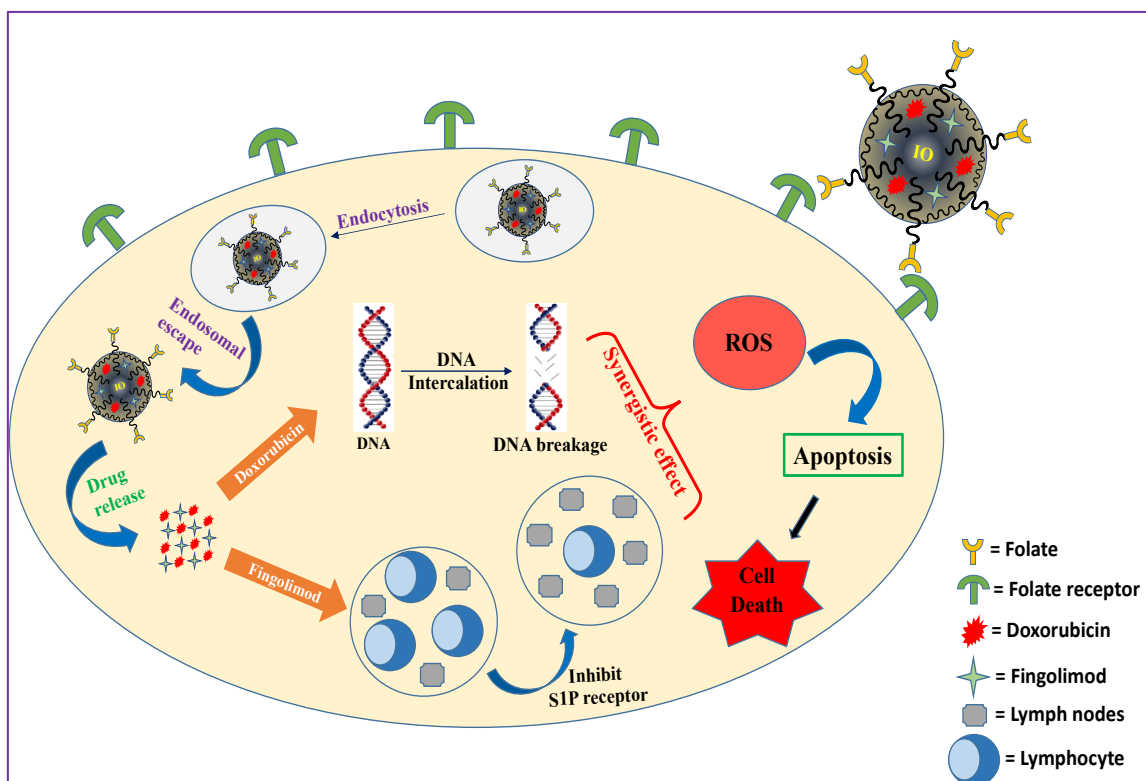


Figure 9: Schematic representation of a combination approach to treat A549 lung cancer cells. The figure represents the endocytosis of IONP-Fol-Doxo-Fingo and the action of drugs on cells.

The chemotherapeutic drug doxorubicin has been used for prostate, stomach and breast cancer treatment since the food, and drug administration approved it in 1995. Doxorubicin interferes with topoisomerase II.⁵⁰ Also, it undergoes numerous actions like interaction with DNA using intercalation and inhibition of macromolecule biosynthesis. One of the most powerful functions of doxorubicin is to target several tissues to yield cytotoxicity, and DNA damage.^{51,52} The structures of doxorubicin and fingolimod are shown in **figure 10A-B**, respectively.

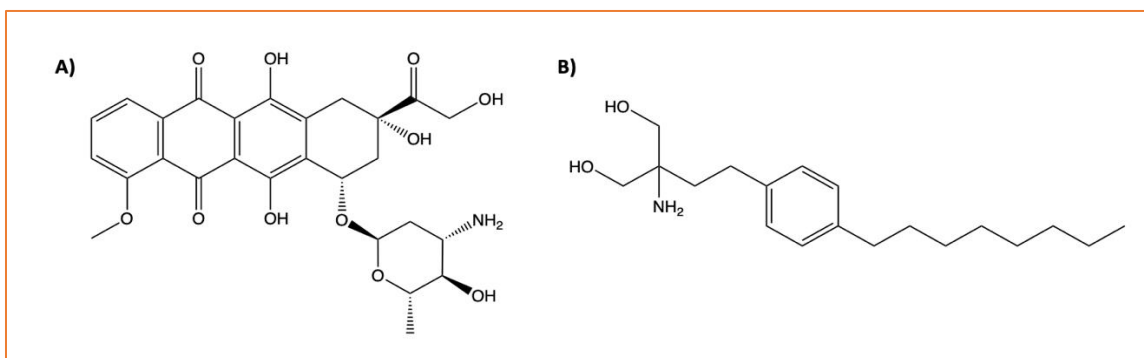


Figure 10: Structural formula of the drugs; A) Doxorubicin, B) Fingolimod.

Fingolimod is a medically approved biological therapeutic drug widely used for multiple sclerosis (MS).⁵³ Fingolimod acts as a hydrophobic and hydrophilic group, which represents its amphipathic nature. Also, it has a robust binding affinity towards the sphingosine-1-phosphate receptor.⁵⁴ The mechanism in which fingolimod employs the therapeutic effect in multiple sclerosis is still unknown. However, the application includes the reduction of the lymphocyte migration into CNS and immunosuppressive drugs for organ transplantation.⁵⁵

Chapter II

Results and Discussion

In this study, polyacrylic acid-coated iron oxide nanoparticles were synthesized by the water-based precipitation method. Targetability was achieved by reacting folic acid with ethylenediamine via carbodiimide chemistry to give folate-amine (Fol-NH₂). Simultaneously, IONPs were co-encapsulated with doxorubicin and fingolimod (**2A-C, Figure 11**). Then, to get the IONP-Fol-Doxo-Fingo (**3A, 1 mM, Figure 11**), folate-amine was added dropwise to the IONP-Doxo-Fingo. A schematic diagram shows the synthesis and design of nanoparticles (**Figure 11**). The doxorubicin's determination in the nanoparticle was confirmed through the UV-Vis spectroscopy due to its fluorescence property. The dynamic light scattering (DLS) studies were taken to measure if size of nanoparticles is appropriate enough to go in and out of the tumor. The zeta potential of the nanoparticles was observed by DLS to confirm functionalization with folate.

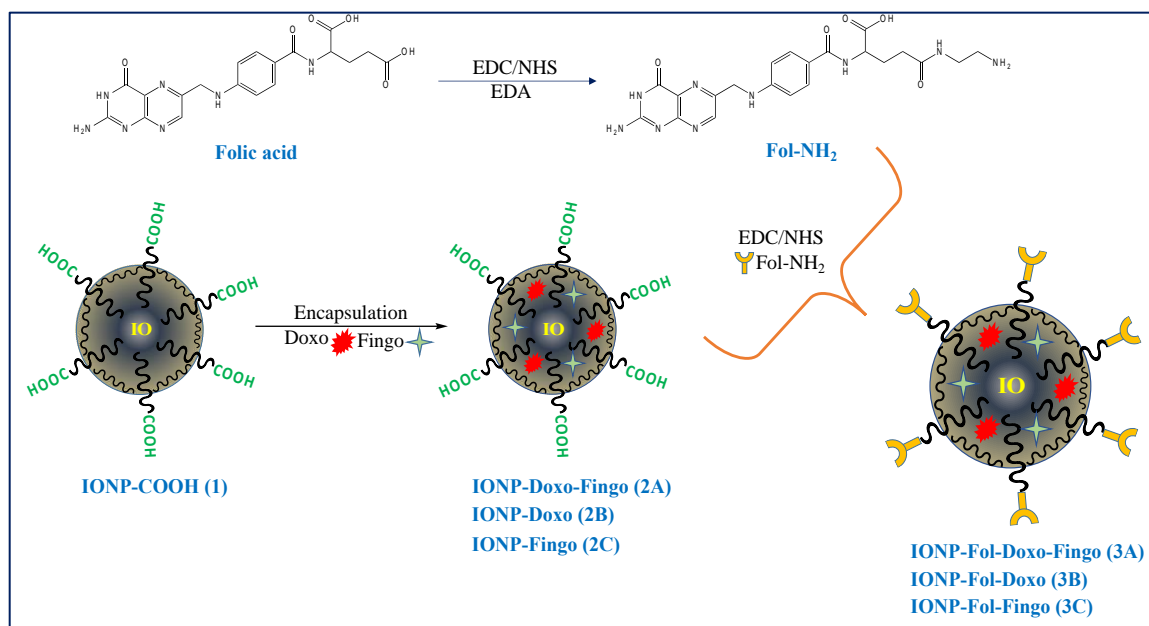


Figure 11: Synthesis of folate functionalized nanomedicine from drug encapsulated iron oxide nanoparticles (IONPs). EDC/NHS chemistry and Solvent diffusion method were used to design nanoparticles.

2.1) Characterization of IONP-COOH:

A water-based precipitation method was used to synthesize the polyacrylic acid (PAA) coated iron oxide nanoparticles, and the surface conjugation was completed by carbodiimide (ECD/NHS) functionalization chemistry (**Figure 11**). After the end of the synthesis, IONP-COOH (**1**, **Figure 11**) was purified by utilizing a magnetic column and, lastly, by dialysis in deionized water (DI water) (dialysis bag MWCO = 6-8 kDa). The magnetic column helps in specifically passing unreacted nonmagnetic reactants, and pure magnetic nanoparticles are acquired. All size and zeta potential were measured using Zetasizer Nano ZS90 from Malvern instruments. The size and zeta potential of purified PAA coated IONP-COOH (4 mM) was measured utilizing dynamic light scattering (DLS). The size of the IONP-COOH was measured to be 50 ± 3 nm (**Figure 12A**), and the relevant zeta potential was found to be -22 ± 1 mV, which confirms the polyacrylic acid coating on the surface of IONP-COOH (**Figure 12B**).

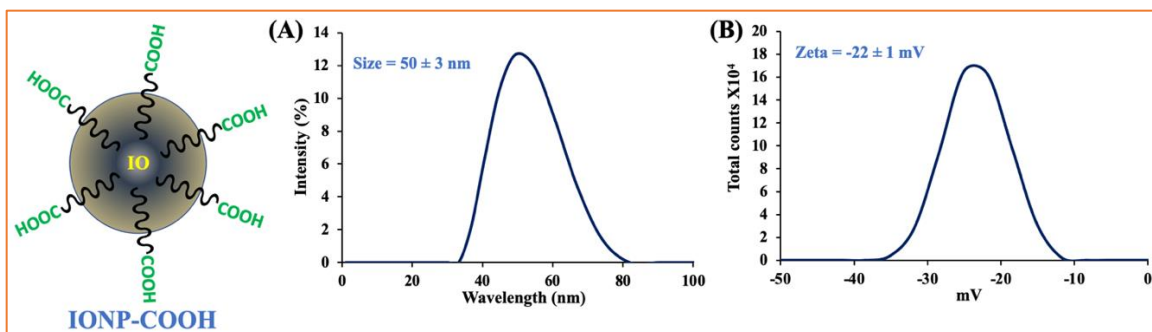


Figure 12: Characterization of IONP-COOH. (A) The size of IONP-COOH was 50 ± 3 nm, and zeta potential was -22 ± 1 mV.

2.2) Characterization of IONP-Doxo-Fingo:

Doxorubicin and fingolimod were encapsulated into IONP-COOH (**1**, **Figure 11**) using the solvent diffusion method to form IONP-Doxo-Fingo (**2A**, 2 mM, **Figure 11**). Size and zeta potential were measured to confirm the presence of drugs in the nanoparticles. The hydrodynamic size of IONP-Doxo-Fingo was found to be 55 ± 1 nm (**Figure 13A**), and the relevant zeta potential was -24 ± 3 mV (**Figure 13B**). The absorbance was measured at $\lambda_{\text{abs}} = 490$ nm (**Figure 13C**), and maximum fluorescence was achieved at $\lambda_{\text{max}} = 600$ nm (**Figure 13D**). The characterization study of IONP-Doxo-Fingo shows successful encapsulation of doxorubicin and fingolimod with iron oxide nanoparticles.

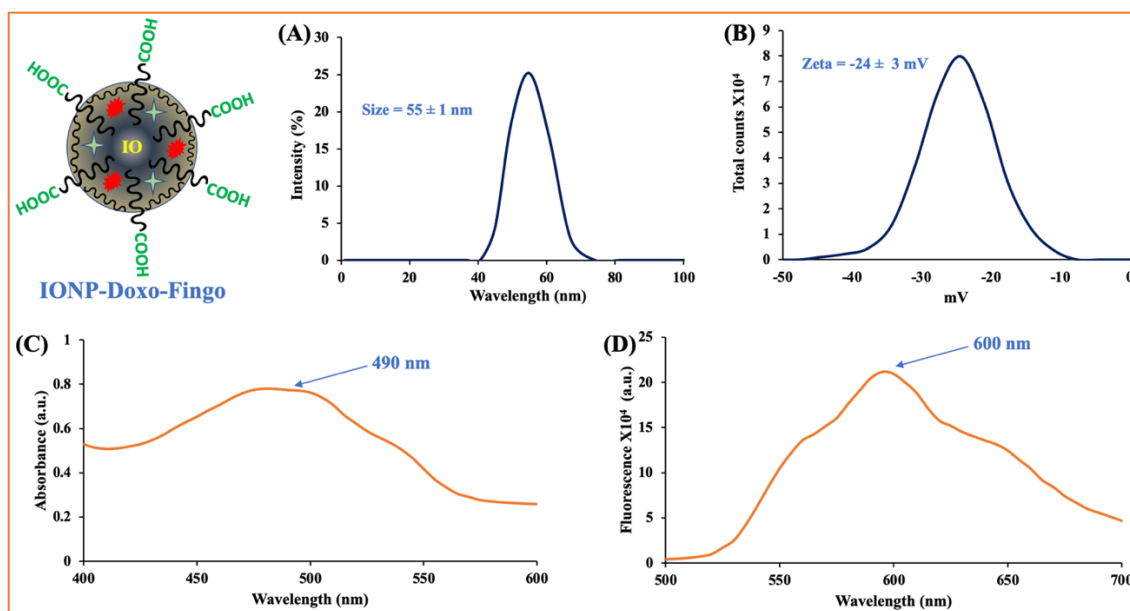


Figure 13: The characteristics of IONP-Doxo-Fingo were studied by dynamic light scattering and UV-Vis spectroscopy. DLS studies showed the size changed to 55 ± 1 nm (A), and the zeta potential was -24 ± 3 mV (B). Spectroscopic studies expressed the absorbance to be $\lambda_{\text{abs}} = 490$ nm (C), and fluorescence was $\lambda_{\text{max}} = 600$ nm (D).

2.3) Characterization of IONP-Fol-Doxo-Fingo:

Next, PAA coated IONPs were functionalized through EDC/NHS chemistry to form IONP-Fol-Doxo-Fingo (3A, 1 mM, **Figure 11**). The hydrodynamic size of IONP-Fol-Doxo-Fingo was observed to be 60 ± 2 nm (**Figure 14A**), and the corresponding zeta potential was -25 ± 2 mV (**Figure 14B**). After conjugation, the size was increased by about 5 nm; the increment in size confirms the folate receptor on the surface of IONPs. Likewise, the change in zeta potential also indicates the surface conjugation of folate on IONPs. The presence of folate was also confirmed via UV absorbance and emission spectroscopy. The maximum absorbance for doxorubicin and folic acid was achieved at $\lambda_{\text{abs}} = 495$ nm and $\lambda_{\text{abs}} = 350$ nm (**Figure 14C**), and the emission spectra found at $\lambda_{\text{max}} = 600$ nm and $\lambda_{\text{max}} = 450$ nm (**Figure 14D**), respectively. Overall, the characterization study of IONP-Fol-Doxo-Fingo (3A, **Figure 11**) indicates successful surface conjugation of folate on the surface of IONP-Doxo-Fingo (2A, **Figure 11**).

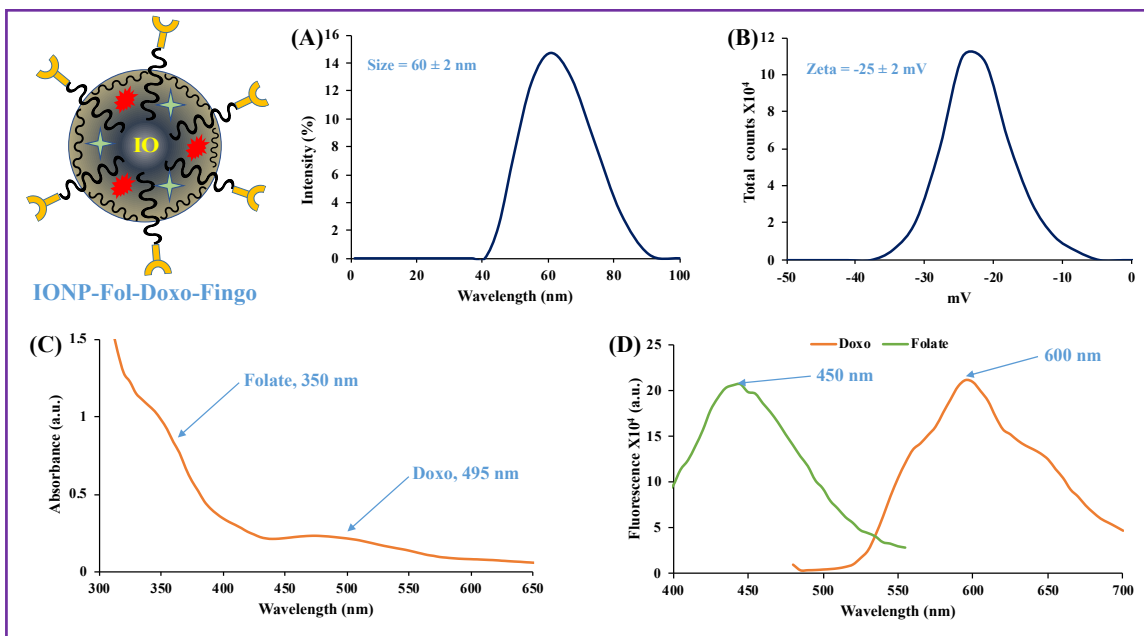


Figure 14: Characterization studies of IONP-Fol-Doxo-Fingo. (A) The hydrodynamic size was found to be 60 ± 2 nm, and the zeta potential was achieved at -25 ± 2 mV (B). Absorbance and emission spectra of folic acid and doxorubicin in nanoparticles (C,D).

2.4) Cytotoxicity studies:

MTT assay is a technique that determines the therapeutic efficacy and cytotoxicity of the compounds. The assay depends on the change of MTT into formazan crystals by active cells, which regulate the mitochondrial activity. The total mitochondrial activity is correlated to the number of live cells in most of the cell population. In other words, the absorbance intensity in purple formazan crystals is directly proportional to the number of living cells. MTT assay is widely used to measure the cytotoxicity of drugs on different cell lines.

Nevertheless, the mitochondrial concentration is small to such an extent in the dead cells that reduction of MTT to its insoluble formazan does not occur. A549 cells were incubated with different drugs such as IONP-Folate, IONP-COOH (1, 4 mM, **Figure 11**), IONP-Folate-Doxo-Fingo (3A, 1 mM, **Figure 11**), IONP-Folate-Doxo (3B, **Figure 11**), IONP-Folate-Fingo (3C, **Figure 11**); to quantify the inhibition proliferation (cell death) via MTT assay. Cell viability of A549 cells was measured for 24 h, 36 h, and 48 h of post-treatment with indicated drugs (**Figure 15**). Figure 15 indicates that at 24 h, individual drugs, doxo and fingo, show 75% and 63% cell viability, respectively. However, drug combination (Comb) delivers 53% cell death in 24 h. Cells treated with IONP-COOH and IONP-Folate showed negligible response throughout the study to

toxicity due to the absence of drugs. At 36 h, the cell viability in IONP-Fingo is higher than that of IONP-Doxo, which means that fingolimod will become less toxic to the cells after 24 h.

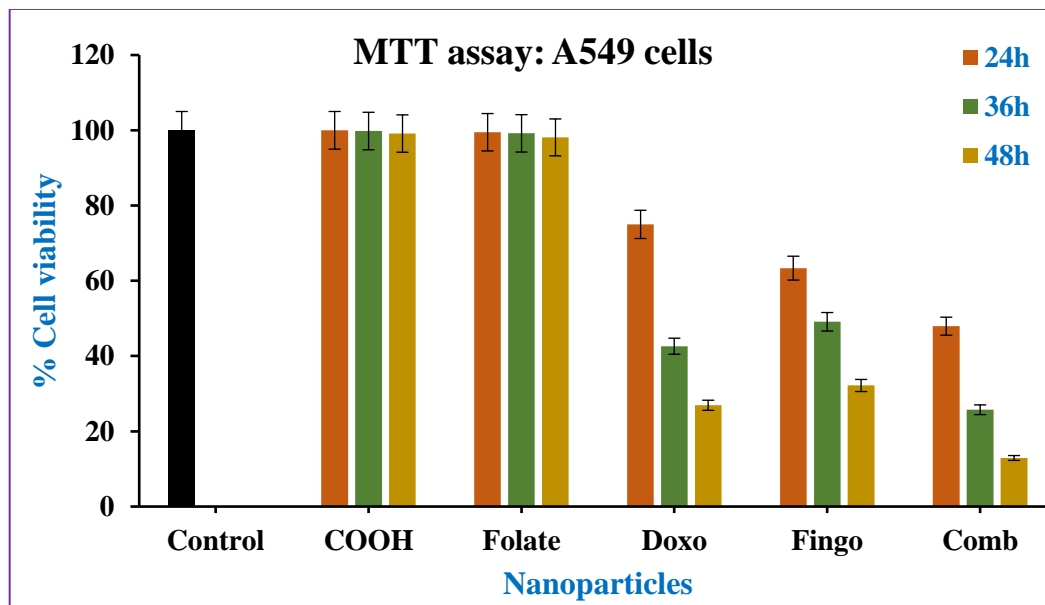


Figure 15: Time-dependent cell viability assay for A549 cells when treated with different nanoparticles. The lowest cell viability or the highest cell proliferation was observed in combination at 48 h.

In comparison with IONP-Fingo, a combination of drugs will have just 25% viable cells. In 48 h, the combination becomes lethal to A549 cells showing only 13% cell viability (87% cell death). This result shows the minimal cell viability and maximum toxicity at 48 h when cells are treated with combined drugs. The sudden decrease in cell viability obtained for IONP-Doxo from 24 h to 48 h is because doxorubicin starts inhibiting with the topoisomerase II to break the DNA strands after 36 h. This synergetic impact in combination with the targeting modality of the folate conjugated IONPs makes powerful treatment while limiting the effects on live or healthy cells that do not overexpress folate receptors.

The MTT assay was also performed to control Chinese hamster ovary (CHO) cells in the same manner. CHO cells are epithelium cell lines derived from the ovary of a hamster. CHO cells do not have a folate receptor on the surface. CHO cells were incubated with IONP-Folate, IONP-COOH (1, 4 mM **Figure 11**), IONP-Folate-Doxo-Fingo (3A, 1 mM, **Figure 11**), IONP-Folate-Doxo (3B, **Figure 11**), IONP-Folate-Fingo (3C, **Figure 11**) for 24 h, 36 h, and 48 h to measure the cytotoxicity of the drugs. As seen in **figure 16**, the drugs show negligible toxicity to cells due to

the receptor's absence on the surface; it cannot bind with the drug. In nutshell, this experiment indicates that formed nanoparticles are specifically targeted to the tumor.

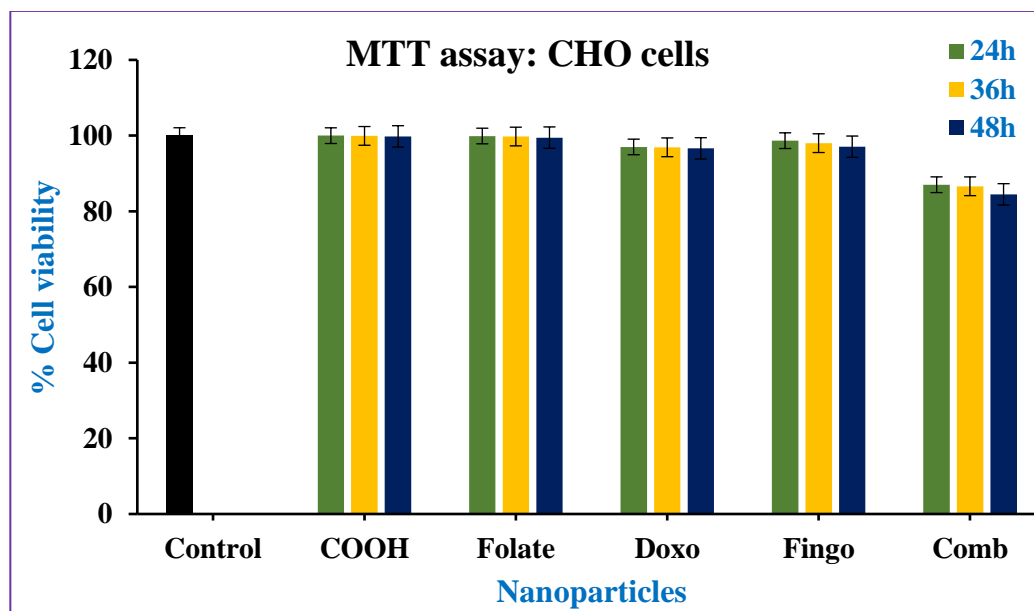


Figure 16: Time-dependent cell viability assay for CHO cells when treated with different nanoparticles. The highest cell viability was observed throughout the study except in combination because of a lack of receptors on the surface.

2.5) Reactive Oxidative Species (ROS) assay:

A better way to accomplish more beneficial anticancer treatment is to improve reactive oxidative species (ROS) levels in cancer cells. The generation of ROS in the cell is measured by dihydroethidium (DHE), a fluorescent dye that is oxidized to 2-hydroxyethidium in the presence of reactive oxygen species and gives red fluorescence after intercalating in DNA. The fluorescence was observed at 24 h, 36 h, and 48 h after treatment. As we go from left to right, the number of cells is dying because increasing treatment time with the drug resulted in a diminution in the number of cells. As seen in **figure 17 A-B**, the live cells with weak ROS intensity were observed after 24 h of incubation. Cell death was observed in MTT assay when A549 cells were incubated with doxorubicin and fingolimod, but more cell death was observed when these two drugs were combined and treated with A549 cells for 48 h (**Figure 17**). In ROS, more cell deaths were observed in 48 h, confirming the result of the MTT assay. Increasing the treatment time resulted in an increase in the red fluorescence intensity, which indicates an increase in ROS generation. The improved strain further demonstrates nanomedicine's synergetic effect and reduced cell number observed at 36 h (**Figure 17 C-D**) and 48 h (**Figure 17 E-F**) after treatment. Overall, these results

indicate successful ROS generation in A549 cells over time when incubated with IONP-Fol-Doxo-Fingo, causing a therapeutic effect.

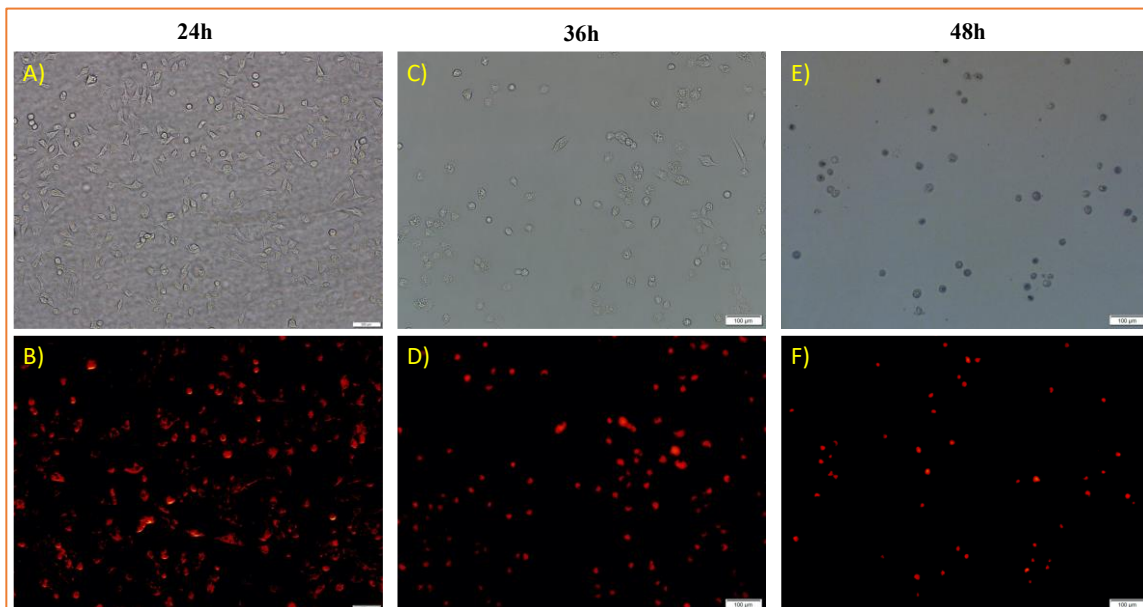


Figure 17: To measure Reactive Oxidative Species (ROS) generation in A549 lung cancer cells were incubated with nanomedicine for 24 h, 36 h, and 48 h. The bright field of reactive species are shown in figure A, C, E and corresponding red filter images B, D, F. (Scale bar 100 μm)

2.6) Cellular apoptosis studies:

The proof of ROS generation provoked the observation of cell death of A549 lung cancer cells. We performed an apoptosis assay to confirm the cell death via apoptotic way. In the apoptotic assay, phosphatidylserine-a phospholipid remains in the cells' internal leaflet transfers to the external leaflet of the cells. Phosphatidylserine is more attracted to a protein. Once this protein attaches to the apoptotic cells, FITC dye-labeled protein (Annexin-V) starts giving fluorescence to the apoptotic cells. Cell apoptosis assay was performed for A549 cells with the treatment of IONP-Fol-Doxo-Fingo (3A, 1 mM, **Figure 11**). These time-dependent studies were taken at 24 h, 36 h, and 48 h. As seen in **figure 18 A-B**, more live cells are present after 24 h of post-incubation. **Figure 18 C-D** indicates that drugs started showing a synergistic effect on the cells after 36 h. The cells are neither completely live nor altogether dead. However, most of the cells were dead after 48 h incubation with nanomedicine (**Figure 18 E-F**). Interestingly, the morphology of A549 cells was changed from branches to a circular shape, indicating apoptosis in the cells. The results signify that nanomedicine is proficient in killing cancer cells.

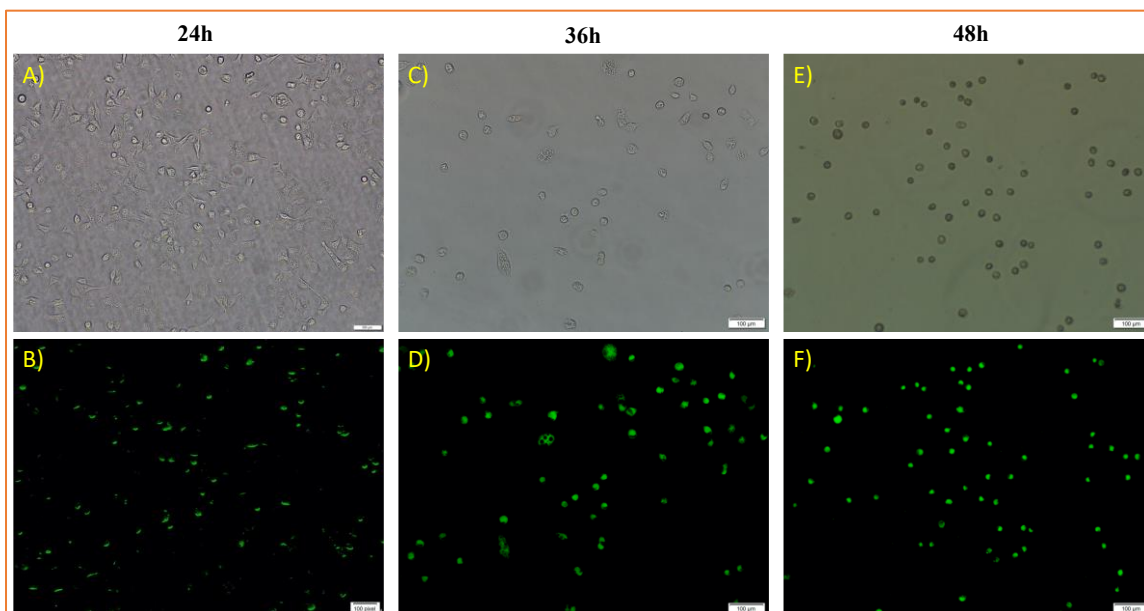


Figure 18: Cellular apoptosis of A549 cells with IONP-Fol-Doxo-Fingo at 24 h, 36 h, and 48 h. A, C, and E are the bright field of apoptotic cells. B, D, and F are green filter images, dye-labeled cells. (Scale bar 100 μm)

2.7) Migration assay:

The transwell migration assay presented here were performed using A549 lung cancer cells. Cell migration is a significant study to focus on cancer research, and it can similarly be applied to development, immunological, and wound healing analyses. Cells were seeded in serum-free media for 24 h in the invasion chamber. After 24 h, cells were treated with PBS (control) showing that most of the cells were migrated to the lower chamber. In contrast, cells were incubated with IONP-Fol-Doxo-Fingo resulted in fewer cells moved to the lower feeder tray. As seen in figure 19, a 4-fold increment in the cells moved toward the chemo-attractant in contrast with the control (**Figure 19**). Overall, the transwell assay resulted that IONP-Fol-Doxo-Fingo has anti-metastatic properties.

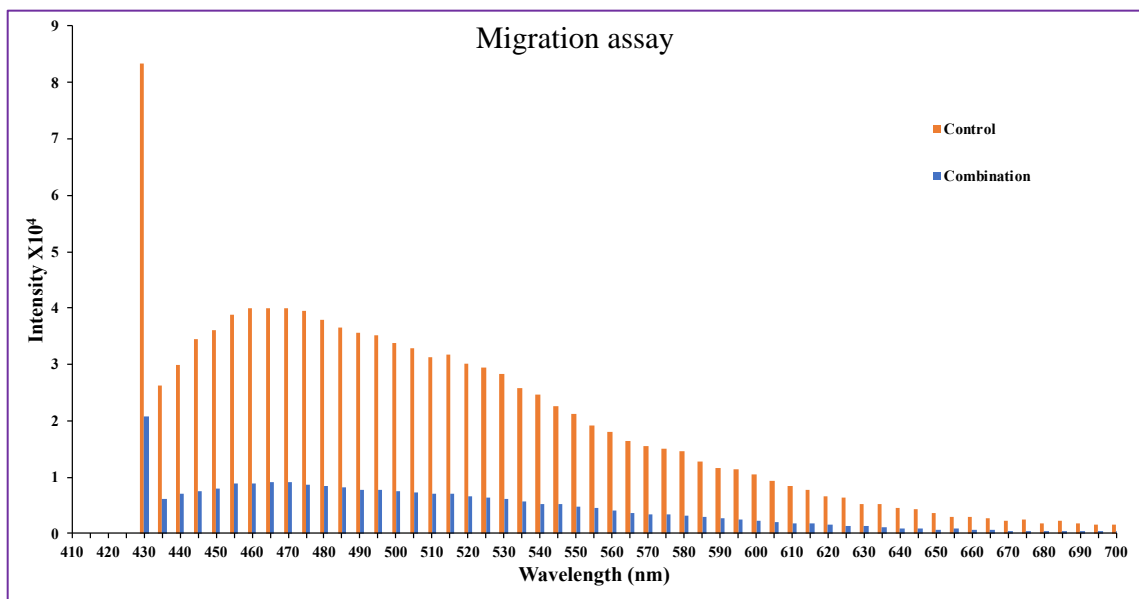


Figure 19: The image shows the anti-metastatic property of IONP-Fol-Doxo-Fingo in A549 lung cancer cells. Control has PBS, and the combination has both the drugs, doxorubicin and fingolimod in IONP-Folate.

Chapter III

Experimental Section

3.1) Materials:

Ferric chloride hexahydrate ($\text{FeCl}_3 \cdot 6\text{H}_2\text{O}$), ferrous chloride tetrahydrate ($\text{FeCl}_2 \cdot 4\text{H}_2\text{O}$), N, N-dimethyl sulfoxide (DMSO), phosphate buffer saline (PBS), ammonium hydroxide (NH_4OH), and hydrochloric acid (HCl) were obtained from Fisher Scientific and stored at an appropriate temperature. 2-morpholinoethanesulfonic acid (MES) and Polyacrylic acid (PAA) were received from Sigma-Aldrich and used without further purification. 4,6-diamidino-2-phenylindole (DAPI) dye was bought from Invitrogen. Apoptosis and necrosis quantification kit (FITC-Annexin V, Ethidium homodimer III and 5X Annexin V binding buffer) was bought from Biotium and stored at 4 °C for future use. Paraformaldehyde was acquired from electron microscopy science. A549 and CHO cells were obtained from ATCC and thawed upon arrival. DMEM, penicillin-streptomycin solution (100X) and fetal bovine serum (FBS) were also acquired from ATCC. Doxorubicin was purchased from Fischer scientific and placed at 4 °C for further use. 1-ethyl-3-(3-(dimethylaminopropyl)carbodiimide hydrochloride (EDC) was obtained from Thermo Scientific, while N-Hydroxy succinimide (NHS) was purchased from ACROS organics and stored at a suitable temperature. Further 3-(4,5-dimethylthiazol-2-yl)-2,5-diphenyltetrazolium bromide (MTT) was purchased from MP bio medicals and stored at 4 °C.

3.2) Synthesis of PAA coated IONPs:

PAA coated iron oxide nanoparticle (IONP) was synthesized using a water-based solvent precipitation method. For preparing PAA coated IONPs, these three solutions were prepared:

1. Iron salts (0.65 mg of $\text{FeCl}_3 \cdot 6\text{H}_2\text{O}$ and 0.35 mg of $\text{FeCl}_2 \cdot 4\text{H}_2\text{O}$) dissolved in 100 μL of 12 N HCl and 2 mL of DI water.
2. Stabilizing agent (0.86 mg of Polyacrylic acid (PAA) dissolved in 5 mL of DI water)
3. An alkaline solution (1.8 mL of 30% NH_4OH in 15 mL of DI water)

The synthesis began with adding an iron salt solution directly to the alkaline solution at 1000 rpm. Next, a stabilizing agent solution was added to the solution, which contains iron salt and

alkaline solution. The mixture was vortex for 60 min at 3000 rpm. The resultant was further centrifuged at 3000 rpm and 4000 rpm for 20 min each. Finally, IONP-COOH supernatant was passed through a magnetic column and dialyzed using a dialysis bag with a molecular weight cut of range 6-8 kDa. Dialysis was performed in a beaker containing DI water and a magnetic stirrer. The water was changed periodically for 24 h, and the purified solution of IONP-COOH (**1**, 4 mM, **Figure 11**) was taken out of the dialysis bag and stored at 4 °C for further use.

3.3) Synthesis of Folate conjugated IONPs:

The IONPs were conjugated with folate using EDC/NHS chemistry. Folic acid was dissolved in 5 mL PBS buffer (pH 7.4). 5 mg of EDC was mixed in 100 μ L MES buffer (pH 6.0) and then added in 2 parts to the solution, which contains folic acid. The solution was mixed appropriately by tilting back and forth for at least 15 seconds. 3 mg of NHS was mixed in 100 μ L MES buffer (pH 6.0) and added in 2 parts to the above-prepared solution. The mixture was mixed accurately by tilting back and forth for 3 min. 2 μ L of EDA mixed in 100 μ L DMSO and then added dropwise to the solution in an interval of 10 seconds between each drop. Later, this mixture was departed on table mixture at 6 rpm for 3 h. This mixture was then taken into a dialysis bag and dialyzed in DI water for 1 hour to eliminate all unreacted particles. Thus, prepared folate-NH₂ solution added dropwise (5 μ L each time) to 2 mL of IONP. This solution was again dialyzed for overnight to extract impurities from the IONP-Folate solution.

3.4) Encapsulation of drugs:

Doxorubicin and fingolimod were co-encapsulated with the folate-coated IONP through the solvent diffusion method. 5 μ L of doxorubicin and 9 μ L of fingolimod were mixed with 200 μ L of DMSO. The combined drug particles were then added dropwise to the 2 mL folate conjugated IONP, mixed with 2 mL of PBS (pH 7.4). The size of the drop added to the solution was 10 μ L each time. The nanoparticles then put on a table mixture for 3 h at 6 rpm. In addition, non-conjugated particles were taken apart using dialysis technique for 1 h.

3.5) Cytotoxicity assay (MTT assay):

To measure the toxicity of the drugs, MTT assay was performed. A549 cells were incubated in 96 well plates for 24 h and stored in an incubator at 37 °C. On the next day, cells were treated with 100 μ L of IONP-Folate, IONP-COOH (**1**, 4mM, **Figure 11**), IONP-Folate-Doxo-Fingo (**3A**, 1mM, **Figure 11**), IONP-Folate-Doxo (**3B**, **Figure 11**), IONP-Folate-Fingo (**3C**, **Figure 11**), and the plates were incubated for 24 h, 36 h, and 48 h. After the treatment time, 30 μ L of 5 mM MTT (3-(4,5-dimethyl-2-thiazoly)-2, 5-diphenyl-2H-tetrazolium bromide) solution was added to

each well and treated for 5 h to allow the formation of purple color formazan. Purple color formazan crystals were solubilized with the help of 75 μ L of acidic isopropyl alcohol. The amount of formazan was measured by changes in absorbance at 570 nm using TECAN infinite M200 PRO plate reader. A similar experiment was also performed for the control cells CHO.

3.6) ROS assay:

For the activity of oxygen species within the cells was measured through ROS assay kit. A549 cells were incubated for 24 h in incubator. After incubation, 100 μ L of IONP-Folate-Doxo-Fingo (**3A**, 1mM, **Figure 11**) was added to the dishes for 24 h, 36 h, and 48 h. After treatment time, cells were rinsed with 1X PBS and stained with DHE dye for 30 min. Then after cells were fixed with 4% paraformaldehyde and images were taken using Olympus IX73 fluorescence microscope.

3.7) Apoptosis assay:

In order to determine the apoptic cells apoptosis quantification kit was used. A549 cells were incubated for 24 h in incubator (37 $^{\circ}$ C, 5% CO₂). 100 μ L of IONP-Folate-Doxo-Fingo (**3A**, 1mM, **Figure 11**) was added to the dishes for 24 h, 36 h, and 48 h. Post treatment period, the cells were washed 2 times with 1X PBS (Phosphate Bovine Serum). Then, 1X binding buffer was added and stained with 5 μ L of FITC dye for 15 min. Cells were washed with 1X annexing binding buffer and fixed with 4% paraformaldehyde for 15 min. These fixed cells were washed again with 1X binding buffer and fluorescence images taken in Olympus IX73 fluorescence microscope.

3.8) Migration assay:

The anti-metastatic property of the cells was analyzed via migration assay. A chemicon QCM 96-well cell migration assay kit from Millipore was used for the experiment. Initially, A549 cells were incubated in serum-free media for 24 h in a big petri dish. Following that, cells were treated with folate conjugated, and drugs encapsulated IONPs (IONP-Fol-Doxo-Fingo; **3A**, **Figure 11**) and PBS for control study. After the treatment time, cells were seeded in the upper invasion chamber for 30 min. Next, the invasion chamber was placed onto a feeder tray containing 10% FBS media and incubated for 24 h to let the cell migrate. The migrated cells were then dislodged from the invasion chamber and placed on a new feeder tray containing cell detachment buffer for 30 min. The cell lysis buffer and CyQuant dye were added to the solution to stain the migrated cells. The fluorescence was taken measured at wavelength 480-530 nm using TECAN infinite M200 PRO plate reader.

Chapter IV

Conclusion and Future Study

IONP-Fol-Doxo-Fingo nanoparticles were successfully synthesized from folate conjugated, and drugs encapsulated IONPs to treat A549 lung cancer. Drugs were encapsulated to give a synergistic effect on tumor cells, and targetability was achieved by folate conjugation on the iron oxide nanoparticles' surface. The theranostic effect of the nanoparticle was confirmed using various cell-based assays. Apoptosis assay proved the drugs' synergistic effect by increasing apoptotic cells from 24 h to 48 h. The migration assay confirmed the anti-metastatic property of the combinations of the two drugs. The nanoparticles were internalized by cancer tumors and successfully released drugs from the vesicle and resulted in 85% cell proliferation after 48 h of incubation. Thus, the combination approach ended up being a successful model for the treatment of lung cancer.

This combination approach can be tailored for specific targeting and various types of cancer tumors such as prostate and breast cancer after such not-specific target-oriented, unstable, and less cell viability treatments available in this area of cancer research. Future works include an in-vivo study of lung cancer to understand better this drug carrier after individual experiments in an in-vitro setting. Therefore, this study of delivering drugs with iron oxide nanoparticles would affect the cancer tumor and help future treatments.

REFERENCES

- (1) <https://www.cancer.org/research/cancer-facts-statistics/all-cancer-facts-figures/cancer-facts-figures-2020>
- (2) WHO. <https://www.who.int/>
- (3) Nguyen J. Targeted nanoparticles for cancer therapy: promises and challenges. *Nanomedic Nanotechnology* **2011**, 2, 5.
- (4) Crino, L., Weder, W., van Meerbeeck, J., & Felip, E. Early stage and locally advanced (non-metastatic) non-small-cell lung cancer: ESMO Clinical Practice Guidelines for diagnosis, treatment and follow-up. *Annals of Oncology* **2010**, 21, 103–115.
- (5) Youlten, D. R., Cramb, S. M., & Baade, P. D. The International Epidemiology of Lung Cancer: Geographical Distribution and Secular Trends. *Journal of Thoracic Oncology* **2008**, 3, 819–831.
- (6) Couraud, S., Zalcman, G., Milleron, B., Morin, F., & Souquet, P.J. Lung cancer in never smokers-A review. *European Journal of Cancer* **2012**, 48, 1299–1311.
- (7) Schiller JH, Harrington D, Belani CP, Langer C, Sandler A, Krook J, et al. Comparison of four chemotherapy regimens for advanced non- small-cell lung cancer. *N Engl J Med* **2002**, 346, 92–8.
- (8) Ramalingam S, Belani C. Systemic chemotherapy for advanced non- small cell lung cancer: recent advances and future directions. *Oncologist* **2008**, 13, 5–13.
- (9) Grossi F, Kubota K, Cappuzzo F, de Marinis F, Gridelli C, Aita M, et al. Future scenarios for the treatment of advanced non-small cell lung cancer: focus on taxane-containing regimens. *Oncologist* **2010**, 15, 1102–12.
- (10) Rebecca L. Siegel, Kimberly D. Miller, Ahmedin Jemal. Cancer Statistics, 2020. *CA Cancer J Clin.* **2020**, 0, 1-24.
- (11) Lammers, T., Kiessling, F., Hennink, W. E., & Storm, G. Nanotheranostics and Image-Guided Drug Delivery: Current Concepts and Future Directions. *Molecular Pharmaceutics* **2010**, 7, 1899–1912.
- (12) Cherian, A. M., Nair, S. V., & Lakshmanan, V. K. The Role of Nanotechnology in Prostate Cancer Theranostic Applications. *Journal of Nanoscience and Nanotechnology* **2014**, 14, 841–852.

- (13) Soppimath, K. S., Aminabhavi, T. M., Kulkarni, A. R., & Rudzinski, W. E. Biodegradable polymeric nanoparticles as drug delivery devices. *Journal of Controlled Release* **2001**, *70*, 1–20.
- (14) Chan, J. M., Valencia, P. M., Zhang, L., Langer, R., & Farokhzad, O. C. Polymeric Nanoparticles for Drug Delivery. *Cancer Nanotechnology* **2010**, *624*, 163–175.
- (15) Wang, Y., & Grayson, S. M. Approaches for the preparation of non-linear amphiphilic polymers and their applications to drug delivery. *Advanced Drug Delivery Reviews* **2012**, *64*, 852–865.
- (16) Bennet, D., & Kim, S. Polymer Nanoparticles for Smart Drug Delivery. *Application of Nanotechnology in Drug Delivery* **2014**. doi:10.5772/58422
- (17) Wang H, Rempel GL. Introduction of Polymer Nanoparticles for Drug Delivery Applications. *J Nanotechnol Nanomed Nanobiotechnol* **2015**, *2*, 008.
- (18) Ferrari, R., Sponchioni, M., Morbidelli, M., & Moscatelli, D. Polymer Nanoparticles for the Intravenous Delivery of Anticancer Drugs: The Checkpoints on the Road from the Synthesis to Clinical Translation. *Nanoscale* **2018**, *10*, 22701-22719.
- (19) O. Flores, S. Santra, C. Kaittanis, R. Bassiouni, Annette R. Khaled, J. Grimm and J. M. Perez. PSMA-Targeted Theranostic Nanocarrier for Prostate Cancer. *Theranostics* **2017**, *7*, 2477-2494.
- (20) Sharma, V., Park, K. & Srinivasarao, M. Colloidal dispersion of Au nanorods: Historical background, optical properties, seed-mediated synthesis, shape separation and self-assembly. *Mater. Sci. Eng. R* **2009**, *65*, 1-38.
- (21) Faraday, M. Michael Faraday's recognition of ruby Au: the birth of modern nanotechnology. *Au Bulletin* **2007**, *40*, 267-269.
- (22) Faraday, M. The Bakerian Lecture: Experimental Relations of Au (and Other Metals) to Light. *Phil. Trans. R. Soc. Lond.* **1857**, *147*, 145-181.
- (23) Mie, G. Contributions to the optics of turbid media, particularly of colloidal metal solutions. *Annalen Der Physik* 1908, *25*, 377–445.
- (24) Baptista, P. et al. Au nanoparticles for the development of clinical diagnosis methods. *Anal. Bioanal. Chem* 2008, *391*, 943-950.
- (25) Liu, X. et al. A one-step homogeneous immunoassay for cancer biomarker detection using Au nanoparticle probes coupled with dynamic light scattering. *J. Am. Chem. Soc.* **2008**, *130*, 2780-2782.
- (26) Luo, P. G. & Stutzenberger, F. J. Nanotechnology in the detection and control of microorganisms. *Adv. Appl. Microbiol.* **2008**, *63*, 145-181.

- (27) Zharov, V., Galanzha, E., Shashkov, E., Khlebtsov, N. & Tuchin, V. In vivo photo acoustic flow cytometry for monitoring circulating single cancer cells and contrast agents. *Opt. Lett.* **2006**, *31*, 3623-3625.
- (28) Das, M., Shim, K.H., An, S.S.A. et al. Review on gold nanoparticles and their applications. *Toxicol. Environ. Health Sci.* **2011**, *3*, 193–205.
- (29) Ajnai, G., Chiu, A., Kan, T., Cheng, C.-C., Tsai, T.-H., & Chang, J. Trends of Gold Nanoparticle-based Drug Delivery System in Cancer Therapy. *Journal of Experimental & Clinical Medicine* **2014**, *6*, 172–178.
- (30) Matsumura Y, Maeda H. A new concept for macromolecular therapeutics in cancer chemotherapy: mechanism of tumorotropic accumulation of proteins and the antitumor agent smancs. *Cancer Research* **1986**, *46*, 6387–92.
- (31) Duncan, R.; Sat Y. N. Tumor targeting by enhanced permeability and retention (EPR) effect. *Ann. Oncol.* **1998**, *9*, 39.
- (32) Vasey PA, Kaye SB, Morrison R, et al. Phase I Clinical and Pharmacokinetic Study of PK1 [N-(2- Hydroxypropyl)methacrylamide Copolymer Doxorubicin]: First Member of a New Class of Chemotherapeutic Agents—Drug-Polymer Conjugates. *Clinical Cancer Research* **1999**, *5*, 83–94.
- (33) Chithrani, B. D., Ghazani, A. A., & Chan, W. C. W. Determining the Size and Shape Dependence of Gold Nanoparticle Uptake into Mammalian Cells. *Nano Letters* **2006**, *6*, 662–668.
- (34) Vallet-Regí, M.; Colilla, M.; Izquierdo-Barba, I.; Manzano, M. Mesoporous Silica Nanoparticles for Drug Delivery: *Current Insights. Molecules* **2018**, *23*, 47.
- (35) Kobler, J., Möller, K., & Bein, T. Colloidal Suspensions of Functionalized Mesoporous Silica Nanoparticles. *ACS Nano* **2008**, *2*, 791–799.
- (36) Argyo, C., Weiss, V., Bräuchle, C., & Bein, T. Multifunctional Mesoporous Silica Nanoparticles as a Universal Platform for Drug Delivery. *Chemistry of Materials* **2013**, *26*, 435–451.
- (37) Wang, Y., Yu, A., & Caruso, F. Nanoporous Polyelectrolyte Spheres Prepared by Sequentially Coating Sacrificial Mesoporous Silica Spheres. *Angewandte Chemie International Edition* **2005**, *44*, 2888–2892.

- (38) Wang, Y.; Yan, Y.; Cui, J.; Hosta-Rigau, L.; Heath, J. K.; Nice, E. C.; Caruso, F. Encapsulation of Water-Insoluble Drugs in Polymer Capsules Prepared Using Mesoporous Silica Templates for Intracellular Drug Delivery. *Adv. Mater.* **2010**, *22*, 4293-4297.
- (39) Cui, J.; Yan, Y.; Wang, Y.; Caruso, F. Templated Assembly of pH-Labile Polymer-Drug Particles for Intracellular Drug Delivery. *Adv. Funct. Mater.* **2012**, *22*, 4718-4723.
- (40) Hudson, S. P., Padera, R. F., Langer, R., & Kohane, D. S. The biocompatibility of mesoporous silicates. *Biomaterials* **2008**, *29*, 4045-4055.
- (41) Lu, J., Liong, M., Li, Z., Zink, J. I., & Tamanoi, F. Biocompatibility, Biodistribution, and Drug-Delivery Efficiency of Mesoporous Silica Nanoparticles for Cancer Therapy in Animals. *Small* **2010**, *6*, 1794-1805.
- (42) Rosen, J. E., Chan, L., Shieh, D.-B., & Gu, F. X. Iron oxide nanoparticles for targeted cancer imaging and diagnostics. *Nanomedicine: Nanotechnology, Biology and Medicine* **2012**, *8*, 275-290.
- (43) Lee, H., Yu, M. K., Park, S., Moon, S., Min, J. J., Jeong, Y. Y. Jon, S. (2007). Thermally Cross-Linked Superparamagnetic Iron Oxide Nanoparticles: Synthesis and Application as a Dual Imaging Probe for Cancer in Vivo. *Journal of the American Chemical Society* **2007**, *129*, 12739-12745.
- (44) Bagalkot, V., Farokhzad, O. C., Langer, R., & Jon, S. An Aptamer-Doxorubicin Physical Conjugate as a Novel Targeted Drug-Delivery Platform. *Angewandte Chemie* **2006**, *118*, 8329-8332.
- (45) Yu, M. K., Jeong, Y. Y., Park, J., Park, S., Kim, J. W., Min, J. J., Jon, S. Drug-Loaded Superparamagnetic Iron Oxide Nanoparticles for Combined Cancer Imaging and Therapy In Vivo. *Angewandte Chemie International Edition* **2008**, *47*, 5362-5365.
- (46) Wang, A. Z., Bagalkot, V., Vasilliou, C. C., Gu, F., Alexis, F., Zhang, L., Farokhzad, O. C. Superparamagnetic Iron Oxide Nanoparticle-Aptamer Bioconjugates for Combined Prostate Cancer Imaging and Therapy. *ChemMedChem* **2008**, *3*, 1311-1315.
- (47) Gupta, A. K., & Gupta, M. Synthesis and surface engineering of iron oxide nanoparticles for biomedical applications. *Biomaterials* **2005**, *26*, 3995-4021.
- (48) Hu, X., & Norris, D. G. Advances in high-field magnetic resonance imaging. *Annu. Rev. Biomed. Eng.* **2004**, *6*, 157-184.

- (49) Gole, A., Stone, J. W., Gemmill, W. R., zur Loye, H. C., & Murphy, C. J. Iron oxide coated gold nanorods: synthesis, characterization, and magnetic manipulation. *Langmuir* **2008**, *24*, 6232-6237.
- (50) Pommier, Y., Leo, E., Zhang, H., & Marchand, C. DNA Topoisomerases and Their Poisoning by Anticancer and Antibacterial Drugs. *Chemistry & Biology* **2010**, *17*, 421–433.
- (51) Tacar, O., Sriamornsak, P., & Dass, C. R. Doxorubicin: an update on anticancer molecular action, toxicity and novel drug delivery systems. *Journal of Pharmacy and Pharmacology* **2012**, *65*, 157–170.
- (52) Fornari FA, Randolph JK, Yalowich JC, Ritke MK, Gewirtz DA. Interference by doxorubicin with DNA unwinding in MCF-7 breast tumor cells. *Mol Pharmacology* **1994**, *45*, 649–56.
- (53) Habibi, M., & Kuttab, H. M. Management of multiple sclerosis and the integration of related specialty pharmacy programs within health systems. *American Journal of Health-System Pharmacy* **2016**, *73*, 811–819.
- (54) Hopkins, C. R. ACS Chemical Neuroscience Molecule Spotlight on Gilenya (Fingolimod; FTY720). *ACS Chemical Neuroscience* **2011**, *2*, 116–117.
- (55) Budde, K., Schütz, M., Glander, P., Peters, H., Waiser, J., Liefeldt, L., Böhrer, T. FTY720 (fingolimod) in renal transplantation. *Clinical Transplantation* **2006**, *20*, 17–24.